Received: October 24, 2014 Revised: February 13, 2015 Accepted: February 23, 2015

(onlinelibrary.wiley.com) DOI: 10.1111/ner.12296

Subject-Specific Multiscale Modeling to Investigate Effects of Transcranial Magnetic Stimulation

Brian D. Goodwin, PhD*; Christopher R. Butson, PhD*†1

Objective: Transcranial magnetic stimulation (TMS) is an effective intervention in noninvasive neuromodulation used to treat a number of neurophysiological disorders. Predicting the spatial extent to which neural tissue is affected by TMS remains a challenge. The goal of this study was to develop a computational model to predict specific locations of neural tissue that are activated during TMS. Using this approach, we assessed the effects of changing TMS coil orientation and waveform.

Materials and Methods: We integrated novel techniques to develop a subject-specific computational model, which contains three main components: 1) a figure-8 coil (Magstim, Magstim Company Limited, Carmarthenshire, UK); 2) an electromagnetic, time-dependent, nonhomogeneous, finite element model of the whole head; and 3) an adaptation of a previously published pyramidal cell neuron model. We then used our modeling approach to quantify the spatial extent of affected neural tissue for changes in TMS coil rotation and waveform.

Results: We found that our model shows more detailed predictions than previously published models, which underestimate the spatial extent of neural activation. Our results suggest that fortuitous sites of neural activation occur for all tested coil orientations. Additionally, our model predictions show that excitability of individual neural elements changes with a coil rotation of ±15°.

Conclusions: Our results indicate that the extent of neuromodulation is more widespread than previous published models suggest. Additionally, both specific locations in cortex and the extent of stimulation in cortex depend on coil orientation to within ±15° at a minimum. Lastly, through computational means, we are able to provide insight into the effects of TMS at a cellular level, which is currently unachievable by imaging modalities.

Keywords: Computational model, motor cortex, neural activation, neuromodulation, transcranial magnetic stimulation

Conflict of Interest: Dr. Butson has served as a consultant for Intelect Medical, NeuroPace, Advanced Bionics, St. Jude Medical, and Boston Scientific. Dr. Butson is also a shareholder of Intelect Medical and is an inventor of several patents related to neuromodulation therapy. Dr. Goodwin has nothing to disclose.

INTRODUCTION

Transcranial magnetic stimulation (TMS) is a method that has been used to noninvasively modulate neural activity in the brain. During TMS, a coil of wire encased in a wand is held to the head and energized by the discharge of a bank of capacitors. Electric current flows in the coil windings, producing a magnetic field normal to the plane of the coil. Magnetic fields are not deflected or attenuated by biological tissue and therefore penetrate the skull and the brain, causing currents to flow by the principle of induction. The resulting current densities can have immediate modulatory effects on neural elements (somas, axons, or dendrites) in much the same way as currents applied directly to the brain using surface or implanted electrodes. TMS is attractive because it is noninvasive, has a good safety record (1), and has been shown to be effective for a range of conditions, including depression (2), epilepsy (3,4), and tinnitus (5). It has also been used as a neurophysiological tool, and several studies over the last 20 years have demonstrated its physiological effects and its potential for improving our understanding of the nervous system (6–10).

However, the use of TMS as a therapeutic or neurophysiological tool has preceded a thorough scientific understanding of its effects. Despite its overall promise, it is limited by considerable variability in physiological response within and among subjects. As a result, it is difficult to predict the response(s) to TMS on an individual patient basis. The variability in the physiological response to TMS could be due to a wide range of factors, including coil position and orientation relative to the head, the stimulation waveform (e.g., monophasic or biphasic), individual anatomical variations, and the neurophysiological state of the subject (11). Our understanding of the effects of TMS is limited by the inability to quantitatively describe the effects and locations of stimulation within both cortex and deeper structures such as white matter (WM).

Address correspondence to: Christopher R. Butson, PhD, Department of Bioengineering, 72 South Central Campus Drive Warnock Engineering Building, Room 3686 Salt Lake City UT 84112 USA. Email: butson@sci.utah.edu

* Marquette University, Milwaukee, WI, USA; and
† Medical College of Wisconsin, Milwaukee, WI, USA

For more information on author guidelines, an explanation of our peer review process, and conflict of interest informed consent policies, please go to http://www.wiley.com/bw/submit.asp?ref=1094-7159&site=1

[1] Current address: University of Utah, Salt Lake City, UT, USA

Currently, there is some debate about the sites of neural modulation resulting from suprathreshold TMS. It is well accepted that pyramidal cells are one of the neural targets of TMS (12). Stimulation of pyramidal cells could occur within the soma (13,14), descending axon (13), or both. The neural response most likely varies relative to stimulation parameters (8). Evidence exists for pyramidal cells as the origin of direct-waves (D-waves), which elicit robust motor responses (such as muscle twitches) during motor cortex stimulation. Contrary to electrical stimulation (e.g., direct cortical electrical stimulation [DCES] and deep brain stimulation [DBS]), TMS threshold stimuli for indirect waves (I-waves) are lower than that for recruiting D-waves (15,16). Evidence suggests that D-waves are recruited by the activation of WM, which results in ascending and descending action potentials that innervate cell bodies and distal interneurons (17,18). The effects of the D-wave can be observed by motor cortex TMS at intensities above resting motor threshold (RMT), and the amplitude of the motor evoked potential (MEP) can be measured by electromyography (EMG).

The mechanisms of stimulation outside the motor cortex are mostly unknown as the majority of our knowledge has been gathered from electrophysiology recordings from descending corticospinal neurons and terminal muscles (8). Describing the neural targets of TMS remains a challenge due to limitations in functional imaging and the inherent diffuseness of stimulation. Compared with implanted electrodes, TMS is relatively nonfocal. Imaging modalities such as functional magnetic resonance imaging (fMRI) (19) and positron emission tomography (PET) (20) have been employed for locating affected areas. However, functional imaging modalities lack the temporal resolution required to observe the immediate effects of TMS. TMS studies combined with electroencephalography (EEG) aim to examine the immediate responses of TMS, but are largely interrupted by the robust stimulation pulse artifact. Even in the absence of artifact, the immediate neural response diffuses throughout the scalp and is mixed with the dynamic responses from the large surrounding region of cortex.

Computational Modeling

Computational models have been used to predict and visualize many types of neuromodulation therapy (21,22). Detailed models can provide imaging of dynamics that are impossible to record with neuroimaging modalities alone. Computational approaches are more frequently employed in neuromodulation because of their ability to make predictions and gain insight into modulatory mechanisms. For example, subject-specific models for DBS have shown efficacy in predicting patient outcomes by analyzing the neural response to electric fields (E-field) produced by DBS electrodes (22). Predictive models, such as this DBS model, integrate anatomical and functional imaging with finite element methods (FEMs) and detailed neuron modeling.

The large parameter space for TMS (stimulus intensity, pulse waveform, pulse frequency, coil geometry, coil placement relative to cortex, coil orientation, etc.) makes computational modeling an attractive approach for better understanding its effects. Past efforts to elucidate the effects of TMS have relied on FEM (23–29). These studies have led to a number of hypotheses about the mechanisms for neuromodulation at the interface of the brain and the electromagnetic field elicited by TMS (15,25). Detailed computational models have confirmed that the effects of TMS depend on nonhomogenous properties of the brain and surrounding cerebrospinal fluid (30). Even the morphology of the pial surface has mechanistic significance pertaining to excitation during TMS, and estimating locations of activation requires realistic field calculations combined with detailed neural models (29).

The fundamental goal of this project was to predict and visualize the neural targets of TMS within a target region of cortex on a subject-specific basis. Our approach is similar to that of past models for TMS (31), where we integrate functional and anatomical imaging data to generate a subject-specific finite element mesh of the whole head. The novel aspect of our experiments is the enhanced detail of cortex and WM we obtained by including multicompartmental pyramidal cells and descending axons. This detailed cell model is an adaptation of a previously published multicompartmental model of a pyramidal cell (32) (Fig. 1; image C). Our method integrates finite element modeling and a computational neuron model to predict the neural targets of single-pulse TMS. The scope of this project is limited to the elicitation of D-waves by single-pulse TMS. Using this computational approach, we aimed to provide a basis to realize the immediate effects of TMS, including: 1) reasons relating to the

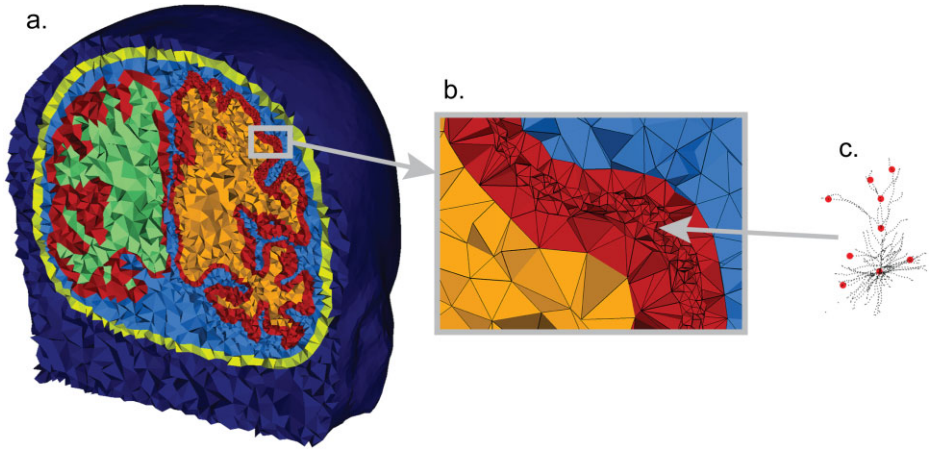

Figure 1. Finite element model. a. A FEM head model was generated from an MRI and segmented into several tissue types. A coronal slice through the FEM is shown with colors indicating the different domains within the mesh: WM (right—green; left—orange), GM (red), CSF (light blue), skull (yellow), and scalp (blue). b. Close-up of GM with high mesh density for regions containing pyramidal cell models. c. Cell body of pyramidal cell neuron model (axon not shown). The black dots indicate biophysical compartments for simulating intracellular response and the red dots indicate the nodes of the cell that are represented in the mesh, which causes higher mesh density in areas of the GM where the neurons exist. CSF, cerebral spinal fluid; FEM, finite element method; GM, gray matter; MRI, magnetic resonance imaging; WM, white matter.

variability in physiology response; 2) diffuseness of excitation; and 3) sites of depolarization within cells across the targeted cortical region.

We designed our modeling process to be tightly integrated with TMS navigation systems, which provide image-guided placement of the coil relative to the subject's brain. TMS navigation is achieved by loading the subject's magnetic resonance imaging (MRI) volume into the navigation system and using real-time optical sensors on the subjects' head (e.g., a headband) and the TMS coil to determine the coil location relative to the brain. TMS navigation is believed to provide more accurate coil placement than using skull landmarks, which helps to minimize inaccuracies during stimulation by "aiming" the induced E-field. During TMS, the patient typically moves his or her head at least millimeters relative to the coil, which changes E-field orientations within the brain and likely foci of neural modulation. We applied our model to assess neural response relative to changes in coil orientation as would be recorded by navigation systems.

TMS shows promise as a neurophysiological tool, but it is limited by the current inability to quantitatively describe precise locations in cortex that are sensitive to TMS stimuli. For this study, we focused our attention on motor cortex stimulation due to its immediate measurable physiological response. Furthermore, complex cortical activity (e.g., direct and indirect waves) can be observed using this approach (33,34).

METHODS

Our computational approach was designed to achieve two primary objectives. First, a prediction of the electromagnetic field in the brain using a model that can easily accommodate changes in biophysical parameters and coil position without the need to recreate the FEM mesh. This prediction facilitates testing a wide range of material properties (e.g., tissue conductivity and nonhomogeneity) and TMS parameters (coil position, orientation, stimulation waveform, etc.). Second, assess the effects of changes in these parameters on the D-wave threshold stimulus of model pyramidal cell neurons in cortex. Simulating neuromodulation during TMS required the use of three primary model components:

1. Model of the figure-8 TMS coil to estimate the magnetic field produced during stimulation.
2. Subject-specific head FEM (Fig. 1) to model the time-dependent electromagnetic field produced in the head. We employed a novel Fourier FEM solver to obtain the time-dependent electromagnetic field within the head.
3. A population of cortical pyramidal cell model neurons that are oriented perpendicularly to the pial surface and are modulated during TMS.

Figure-8 TMS Coil Field Model

The effects of TMS depend on both fixed and adjustable parameters. Fixed parameters include coil geometry and the number of coil windings. Adjustable parameters include the coil position, coil orientation (θ), stimulus intensity, and stimulus waveform. In order to increase computational efficiency, we developed a technique that requires only the head to be included in the FEM mesh, which avoids meshing of the coil and surrounding air (31).

To avoid having to include magnetic induction sources within the mesh, we designed a figure-8 coil model that analytically computes the magnetic vector potential (A-field, Wb/m) using a custom MATLAB script (MathWorks Inc., Natick, MA, USA). This model computes the A-field (at any point[s] in space) from the figure-8 coil using superposition (Fig. 2), and it is specifically designed for computing the A-field boundary condition on the surface of the scalp. Coil geometry (coil inner/outer diameter of coils, centroid of coils, number of windings, winding thickness, and coil height) was based on x-ray measurements of the coil (35). Our TMS-coil model was designed specifically to approximate the figure-8 coil windings by using current dipoles (Q, A*m) as shown in Figure 3. The A-field was computed from

$$\vec{A}_i = \sum_j \vec{Q}_j \mu_0 / 4\pi R_j \quad (1)$$

where μ_0 is magnetic permeability of free space and R_j is the distance between the location of each current dipole Q_j and a point in space. The coil orientation is defined as the angle between the coil handle and the interhemispheric fissure. Current dipoles of the

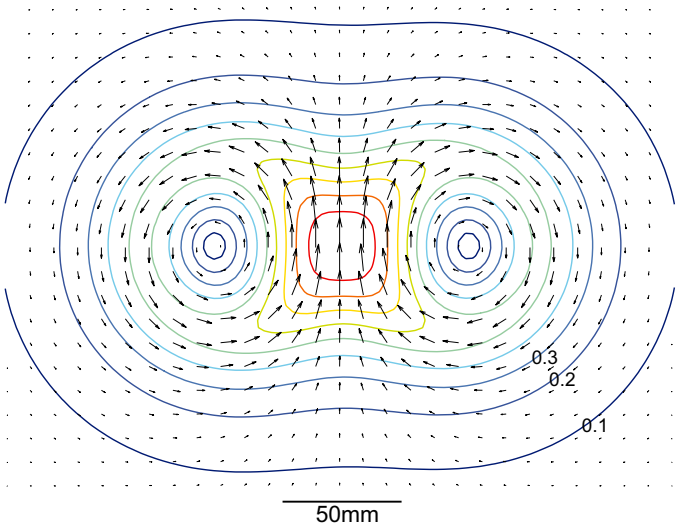

Figure 2. Induced A-field vectors and magnitude contour map. Induced A-field vectors and relative A-field magnitude contour lines in free-space on a plane 1 cm below the plane of the figure-8 TMS coil. Dark red line indicates 0.9 of the max E-field magnitude.

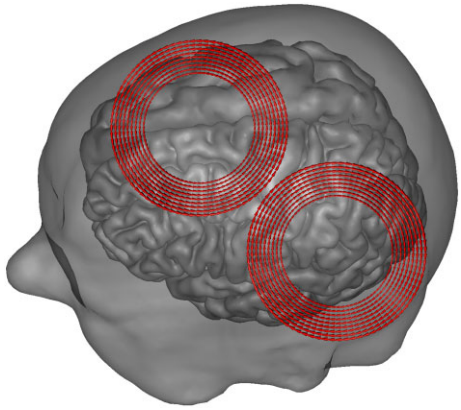

Figure 3. TMS coil model. The TMS coil is approximated by current dipoles that represent the wire windings; each red arrow represents a single dipole. This image shows the representation for a coil position of 45° above the hand-knob of the motor cortex.

figure-8 coil with a 45°-coil orientation are shown in Figure 3, which is typical for motor cortex stimulation. We adopted the orientation and coordinate frame from clinical neurophysiology.

In this study we characterized the effects of the figure-8 coil. Though our approach is amenable to constructing coil geometries of any kind (H-coil, cloverleaf coil, etc.) (36,37), we chose to employ the figure-8 coil as it is more widely used than any other commercially available coil geometry.

Subject-Specific Finite Element Head Model

A subject-specific FEM was generated from an MR image volume acquired from a healthy adult subject. The whole-head T1 MR image was acquired on a 3T scanner (General Electric, Fairfield, CT, USA) at $0.86 \times 0.86 \times 1$ mm voxel resolution ($217 \times 251 \times 180$ voxels). Individual tissue types were segmented from the high-resolution anatomical MRI volume using Brainstorm (38) and FreeSurfer (39). The Iso2Mesh toolbox (Martinos Center for Biomedical Imaging, Massachusetts General Hospital/Harvard Medical School) was used with MATLAB (MathWorks Inc.) to generate a tetrahedral mesh of the head. Though conductivities of biological tissues are debatable and the thickness of cerebral spinal fluid (CSF) spaces varies among subjects (40), we applied "typical" isotropic conductivity values to the head model based on mean values from multiple studies (41). Our subject-specific head model contains white matter (WM), gray matter (GM), CSF, skull (42), and scalp (42), with isotropic conductivities of 0.126, 0.276, 1.654, 0.010, and 0.465 S/m, respectively (14,31). The head model was discretized into approximately 1.75 million tetrahedral elements.

The FEM method for electromagnetodynamics is well established (43). We employed the *Magnetic and Electric Fields* physics module within COMSOL Multiphysics version 4.3 (COMSOL Inc., Burlington, MA, USA) to solve the electromagnetic fields within the conductive FEM. The electromagnetic field equations were solved using an FGMRES (Flexible Generalized Minimum RESidual) iterative solver. Our approach enables the FEM solver to converge toward the time-varying electromagnetic field solution under any TMS parameters using the same discretization. Ampere's law with current conservation was applied to all domains within the model. The A-field was applied as the boundary condition on the outermost boundary (scalp) as computed using the Figure-8 TMS coil model. The resulting magnetic field that permeates the head is computed within the COMSOL Multiphysics solver.

We strategically limited our study to target only the hand-knob area of the motor cortex. The hand-knob is relatively easy to identify and allows for ease of comparisons between model simulations and physiology. Furthermore, the hand-knob is commonly used in TMS research as a landmark for TMS to approximate the location of target regions as well as the tuning parameters such as the RMT. The hand-knob is also used to measure changes in cortical excitability due to an immediately observable response (34,44–47).

Fourier Solver

The E-field produced during TMS is dependent on the location of the coil relative to the brain, as well as the stimulation waveform. We adapted a time-dependent Fourier Solver originally developed by Butson et al. (22) for use in FEM. Our Fourier Solver is designed to solve an electromagnetic field problem from the input of a time-variant stimulus waveform that describes the electric current flow through the coil. The time-dependent solution for the E-field is obtained in three steps (arrows in Fig. 4): 1) calculating the discrete Fourier transform (DFT) of the coil-current stimulation waveform; 2) solving the FEM at each Fourier component; and 3) calculating the inverse discrete Fourier transform (IDFT). We assumed that tissue is purely resistive, computed the electromagnetic FEM at a single frequency (1 kHz), and used the Fourier Solver to obtain the ratios of the maximum E-field from the TMS waveforms to the E-field computed at 1 kHz. These ratios were 2.65:1 and 2.97:1 for the (normalized) monophasic and biphasic waveforms, respectively. Because this ratio is sufficient to compute the maximum E-field when permeability and permittivity effects are negligible, the FEM need not be solved at all frequencies in the TMS waveform spectrum.

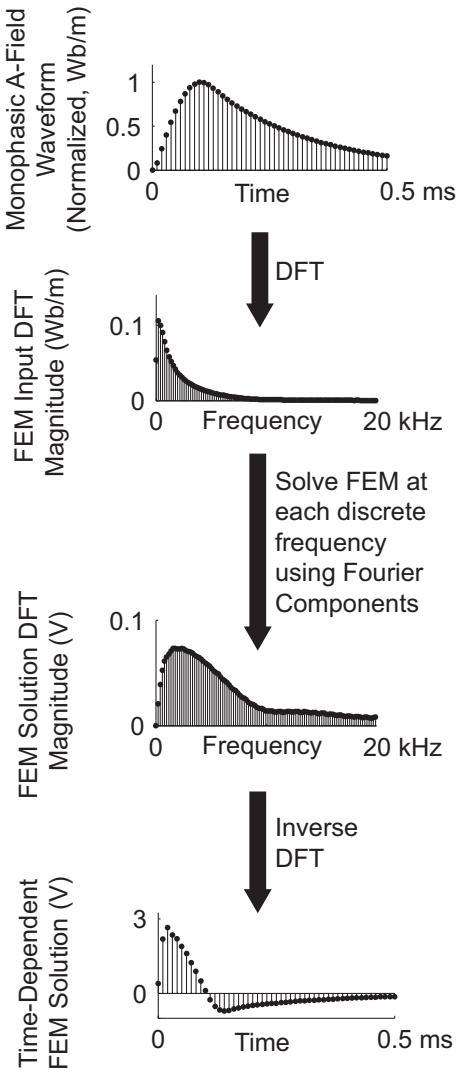

Figure 4. Fourier FEM solver flow diagram. The Fourier FEM solver was used to determine the time- and space-dependent voltage in the brain. From top to bottom: 1) the time-dependent monophasic A-field is calculated from the coil model and is applied as the boundary source condition to our FEM; 2) the FEM is solved at each of the DFT components, which results in the DFT components of the electromagnetic solution; 3) the time-dependent solution to the electromagnetic FEM is then obtained by taking the inverse DFT of the DFT components of the electromagnetic solution. DFT, discrete Fourier transform; FEM, finite element method.

Neuron Model

We implemented a biophysically based model of a pyramidal cell located in cortex. We adapted a model originally created by

Amatrudo et al. (32) using the NEURON simulation environment (Yale, New Haven, CT, USA). This model was chosen based on the microstructure of a real pyramidal cell from layer 3 dorsolateral prefrontal cortex (dlPFC) in a rhesus monkey brain and its biophysical properties. This pyramidal cell model is made up of >1000 neuron compartments wherein biophysical properties are defined. We elected to employ pyramidal cell models on the basis that pyramidal cells are one of the primary stimulation targets during TMS. The pyramidal cell model was adapted to include extracellular mechanisms in which the cell responds to an externally applied, time-dependent E-field (obtained from head FEM). The total E-field solution from the FEM was directly applied to each neuron through NEURON's extracellular mechanism (Fig. 5). We embedded a custom D-wave threshold finder, which searches for the minimum stimulus amplitude to cause either direct or indirect (e.g., action potential initiation within the axon) depolarization of the soma of the pyramidal cell (48). With this design, it is also possible to record the location of action potential initiation on the neuron and the time-dependent response of every compartment in the neuron model for any possible TMS waveform.

The neuron threshold was computed relative to the dial as indicated on the stimulator unit. We obtained *in vitro* recordings of the electromotive force induced from each stimulator unit (Magstim 200 and Magstim Rapid, Magstim Company Limited, Carmarthenshire, UK) in order to find the ratio between the maximum-induced E-field between the two waveforms (monophasic and biphasic). The maximum E-field ratio was approximately 1:0.6 for monophasic to biphasic. Consequently, the thresholds from monophasic stimulation tended to be lower than those from biphasic stimulation because the maximum E-field output from the Magstim Rapid stimulator unit is about 60% of that from the Magstim 200 stimulator unit.

Cortex Model

We modeled a patch of cortex using replicates of the pyramidal cell and its axon. Axons of each pyramidal cell were modeled to simulate realistic axons projecting normally from the GM and curving into the WM. The pyramidal cell model was replicated about 2000 times within the GM in both the targeted and surrounding untargeted regions of the cortex (Fig. 5). The targeted region is indicated by the red surface and the untargeted regions of the pial surface by the blue surface in Figure 6. The red and blue surfaces spread ~70 cm (2). For each neuron compartment, the parallel E-field component was computed and "placed" on the neuron to simulate its response. We expected depolarization to occur within the neuron model where the activating function is maximum. In other words, we simulated the response of each neuron (2000 neurons total) to the total E-field produced by the TMS coil throughout the duration of the stimulus for 24 different coil orientations (15° increments). For each pyramidal neuron, the D-wave threshold was found for every tested coil orientation. This quantity provides a description of the "excitability" of corresponding pyramidal cells for any given coil location and orientation. We constructed excitability maps (see Fig. 7) using the D-wave threshold measure. A unique map was generated for each tested TMS coil orientation.

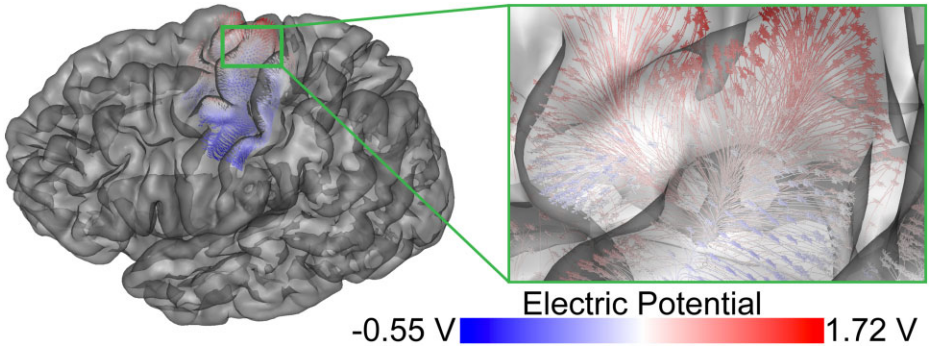

Figure 5. Pyramidal cell models in cortex. Pyramidal cell models with axons are shown inside the transparent pial surface (2000 total neurons). The electric potential (V) solution from the –90° coil orientation is overlaid on the neurons for the purpose of example. Each pyramidal cell has a unique response to extracellular stimulation from TMS for all tested coil orientations. TMS, transcranial magnetic stimulation.

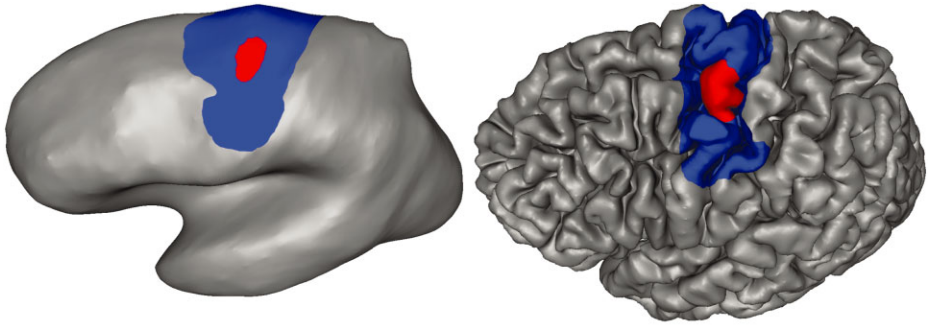

Figure 6. Cortical target region. The folded pial and unfolded (obtained from Freesurfer) pial surfaces are shown with the area being analyzed. Neurons were modeled underneath the cortical areas contained by the blue and red surfaces. The red area contains the hand-knob of the motor cortex, which is the target area. A total of 2000 neurons were modeled underneath the shown colored surfaces.

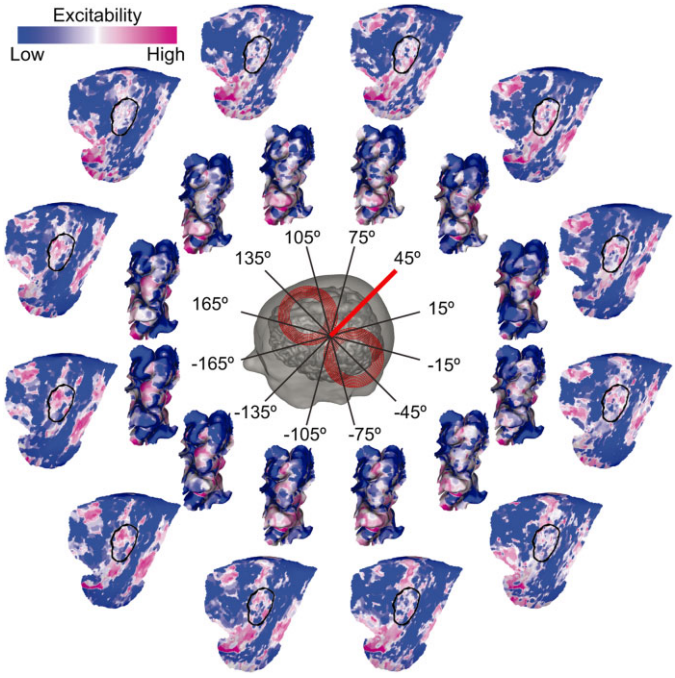

Figure 7. D-wave maps relative to coil orientation. Coil orientations are shown relative to the interhemispheric fissure. At 0°, the coil handle (black lines) is parallel to the interhemispheric fissure and facing posterior. The orientation of red TMS coil is indicated by the red line and is the most common coil orientation for motor cortex stimulation. Each coil orientation has two corresponding surfaces: 1) the folded pial surface containing the targeted and untargeted areas; and 2) the unfolded pial surface containing the exact same map as the folded pial surface with a black outline of the hand-knob region of the motor cortex as shown in Figure 6. "Excitability" describes the D-wave threshold to a monophasic stimulus of the neurons directly underneath a given area of the surface. Areas in pink contained neuron models that possessed low stimulation thresholds, being more excitable than neurons located under blue areas that had high stimulation thresholds. TMS, transcranial magnetic stimulation.

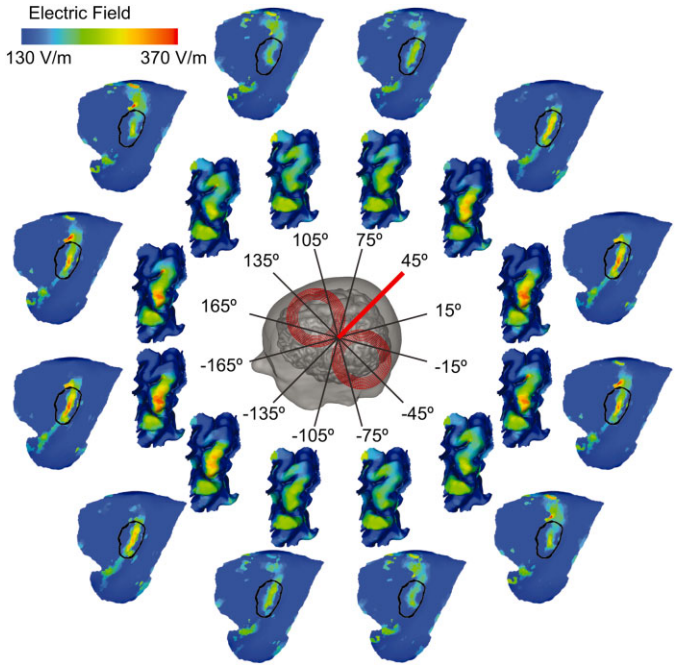

Figure 8. Electric field magnitude maps relative to coil orientation. Coil orientations are shown relative to the interhemispheric fissure. At 0°, the coil handle (black lines) is parallel to the interhemispheric fissure and facing posterior. The orientation of red TMS coil is indicated by the red line and is the most common coil orientation for motor cortex stimulation. Each coil orientation has two corresponding surfaces: 1) the folded pial surface containing the targeted and untargeted areas; and 2) the unfolded pial surface containing the exact same map as the folded pial surface. False color maps show the maximum E-field magnitude induced on the pial surface that results from the monophasic TMS pulse obtained from the FEM. FEM, finite element method; TMS, transcranial magnetic stimulation.

RESULTS

Our modeling approach calculated E-fields far more efficiently than the traditional approach that includes the TMS coil within the FEM mesh. The traditional approach requires an FEM mesh that encompasses the head, coil, and surrounding air space. We found that a mesh of this size requires >3 million elements, and a new mesh must be generated for every change in TMS coil location and orientation, a process that takes about 10 min on a high-end OSX workstation. We designed an equivalent model that requires only a single FEM mesh of the head with ~1.5 million elements, and does not require a new mesh for each coil orientation. The major advantage to this approach is that we can much more easily accommodate changes in coil position, a capability that we believe is necessary for the model to be integrated with TMS navigation systems.

To test the accuracy of our novel approach, we constructed a traditional FEM mesh that contained a spherical model of the head, windings of the TMS coil, and surrounding air in a semi-infinite medium. We compared the electromagnetic solution from the traditional model with our new approach. The mean percent difference between the two solutions was found to be 0.41%, with a standard deviation of 0.29%. The key efficiency improvement came from calculating the A-field, which is an intermediate representation of the magnetic field imposed on the head. However, this A-field calculation is an additional step that is not required for the traditional model, so we next compared the amount of time required to solve the electromagnetic field equations using each approach on a Macintosh workstation (Apple Inc., Cupertino, CA, USA) with quad-core Xeon CPUs (2.66 GHz). We found that the traditional approach required about 1 hour to solve the E-field for each coil position. This amount of time was required to position the coil relative to the head in COMSOL, create the FEM mesh, and solve for the E-field. In contrast, our approach required about 13 min for each coil position and can be automated to solve for multiple coil positions. Using our approach, the FEM mesh was generated once for the head. The TMS coil position was determined using an ANT navigation system; these position data were fed into a custom MATLAB script that calculated the A-field (~10 sec). The A-field was used as a source boundary condition in COMSOL, which calculated the E-field (~11 min). Hence, the additional time to calculate the A-field was offset by the computational time savings provided by creating only a single FEM mesh.

We first assessed electric field magnitudes in the cortical target region as a function of coil orientation. Our results show subtle changes in E-field magnitude inside the targeted area and adjacent gyri as the coil angle θ was varied. The hand-knob gyrus contains the largest E-field magnitudes as θ increases from −15° to +45°. The largest E-fields within the targeted hand-knob were observed with coil orientations where the primary direction of the induced E-field is roughly perpendicular to the central sulcus (between −135° and −165°, and between 15° and 45°) (Fig. 8). Other coil orientations

resulted in lower E-field magnitudes around the targeted region. E-field magnitudes within the WM were found to be comparable with magnitudes observed in the GM. Finally, the E-field magnitudes were identical for opposing coil orientations (e.g., 45° and −135°).

The electric potential solution was obtained via FEM. We then interpolated the electric potential onto pyramidal cell NEURON models replicated within the GM surrounding the targeted area (Fig. 5). The electric potential was obtained from the electromagnetic FEM solutions of each coil orientation. The minimum stimulus intensity required to cause either direct or indirect depolarization of the soma (or D-wave threshold) was computed to measure the excitability of the pyramidal cells. Neurons that had low (below the mean) thresholds were deemed more excitable than areas with high (above the mean) thresholds. D-wave threshold results are represented as a false color map of the pial surface that contained NEURON models directly underneath (Fig. 7). Approximately 2000 neuron models were placed underneath the pial surface. Contrary to E-field maps, excitability maps between opposing coil orientations (180° difference) differed from each other.

Our results confirm past RMT measurements where the most robust motor response is observed when the coil is oriented at 45° (Fig. 9). However, discontinuities exist between excitable areas at 45° and other orientations (Fig. 7). Neurons within the hand-knob (Fig. 6) have high D-wave thresholds for coil orientations between +75° and +135°.

We compared monophasic and biphasic TMS waveforms delivered by stimulator units Magstim 200 and Magstim Rapid (Magstim Company Limited), respectively (Fig. 9). We found that changes in coil orientation similarly affect D-wave thresholds for both monophasic and biphasic waveforms (Fig. 9). Importantly, the maximum E-field required to cause depolarization was generally lesser during biphasic stimulation than during monophasic stimulation.

At 0°-coil orientation, low D-wave thresholds were observed in areas on the posterior side of the hand-knob gyrus. Orientations near 180° elicited low thresholds on the anterior side (Fig. 7). This finding suggests that the location of maximum E-field is a coarse predictor of the location of stimulation from TMS. Electrophysiology studies (30) confirm that threshold values in the hand-knob are sensitive to coil orientation and not just positional placement over the scalp. Our results indicate that a 30°-coil orientation has the greatest excitatory effect whereas an orientation of 150° produces a threshold map with the fewest neurons below mean threshold (Fig. 9).

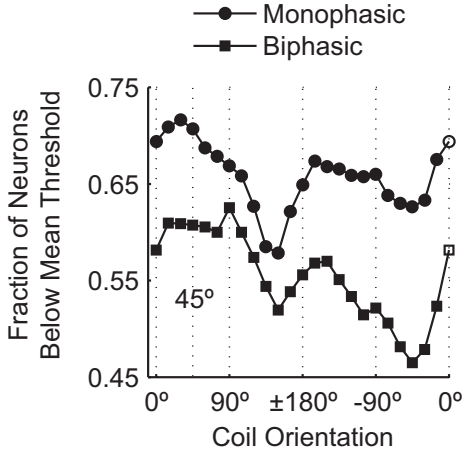

Figure 9. Quantified response for monophasic and biphasic waveforms. Fraction of neurons (out of 2000) for each coil orientation that have stimulation thresholds below the global mean threshold (the mean threshold of all neurons from every coil orientation and each TMS waveform), which we calculated from a total of 96,000 neurons. The biphasic and monophasic TMS waveforms were obtained from *in vitro* recordings from the Magstim Rapid and Magstim 200, respectively. The empty markers on the right side of the plot are copies of the 0° quantities on the far left of the plot. TMS, transcranial magnetic stimulation.

For most neuron response simulations, suprathreshold stimulation elicited an action potential originating in the axon separated by a varying number of nodes of Ranvier from the hillock. Action potentials initiated deeper within the WM or within GM, close to or within the axon hillock. More than 5% of modeled neurons show initiation of two action potentials at different sites along the curved axon.

DISCUSSION

The fundamental goal of this project was to develop and test a methodology that would enable prediction and visualization of possible neural targets of D-wave recruitment within a patch of cortex on a subject-specific basis. To achieve this goal, we developed a detailed subject-specific model that incorporates biophysically based pyramidal cells within and around the targeted area of cortex. We reported computations of the D-wave threshold stimulus and simulations of each neuron response to the threshold stimulus. We built upon past models that have relied on FEM and that used the E-field to predict areas of D-wave recruitment (23–29). Our aim was to use the E-field to realize the immediate effects of TMS, including: 1) reasons for the variability in physiology response; 2) span of excitation; and 3) sites of depolarization within cells in the targeted cortical region.

Electrical stimulation (e.g., DCES, DBS, transcranial direct current stimulation; tDCS) injects charge (current) into the brain (and then retrieves it), which gives rise to an electric potential and causes activation of nearby neurons (49). The E-field gradients elicited from TMS are substantially less than those elicited from electrical stimulation. Consequently, the effects of magnetic stimulation are more dependent on brain anatomy than DCES or DBS. Our approach demonstrates that the use of neuron models and FEM can provide insights into possible mechanisms of magnetic stimulation.

Numerous cell types exist in cortex, but we focused on synaptically isolated pyramidal cells, which mediate D-wave recruitment to TMS of motor cortex (12–14). The current state of our model is only capable of computing D-wave thresholds of pyramidal cells. Even though these neuron models do not account for any presynaptic or interneuron activation, our approach is an important step to characterizing the cellular effects of TMS. Including the effects of TMS on interneurons would almost certainly play a role in the coil angle sensitivity for tissue activation, but only in the case where I-waves are of interest. Future work will include interneurons with synaptic connections to examine postsynaptic effects on pyramidal cells.

Our current subject-specific model accounts for nonhomogeneous, isotropic conductivities. This FEM model currently suffers a major limitation in that its conductivities are only isotropic. Recent research suggests that there are not only anisotropies within WM, but also within GM (50), which could cause TMS to have more focal (and perhaps sparse) effects. Work is currently under way to employ MRI techniques such as diffusion-weighted imaging (DWI) to accurately assign more realistic material properties for each head segment. This approach would allow for the inclusion of anisotropic conductivities. Additionally, a natural limitation of our FEM is the mesh density. However, we chose a mesh density where further

refinements would result in a negligible change in the solution. Because the divergence of the E-field is so small compared with the E-field magnitude, the mesh density to reach this criteria was coarser than needed to simulate implanted electrodes.

Importantly, our modeling results do not have explicit validation, but are based on established computational analyses. Our subject-specific model has several important limitations, but it confirms physiological observations for motor cortex stimulation. Specifically, electrophysiology studies confirm that the most robust response is elicited with a coil orientation that induces current from anterior to posterior (51,52). Our model additionally confirms this physiological phenomenon by quantifying the overall effect of TMS relative to coil orientation (Fig. 9).

We observed a strong correlation between coil orientation and D-wave thresholds across the targeted region (Fig. 9). However, individual maps (Fig. 7) of local thresholds have complex features that make it difficult to draw broad conclusions about activated regions. Here, we expanded upon existing models for TMS by implementing neuron modeling, which has been more frequently used in neuromodulation over the last decade (49,53,54).

Previous studies have simplified the TMS pulse by modeling it as a single fundamental frequency (31). This simplification is valid for electromagnetic theory because permittivity values have negligible effects on the electric field during TMS. Our results indicate that this is an oversimplification of the waveform dynamics in simulating the response of neural elements (see Fig. 7). Our time-dependent model provides insight into the advantages or disadvantages of certain TMS waveforms. We have reported D-wave threshold maps for only the monophasic waveform (Fig. 7), but we have shown comparisons between the effects of mono- and biphasic waveforms (Fig. 9). The TMS waveform shape has an effect on the threshold, and the Fourier Solver provides the means to analyze the effects of any TMS waveform (53,55), including waveform efficiency in terms of power output and neuron threshold. Our subject-specific approach assumes that the effects of permittivity are negligible, and therefore, the relationship is linear between the estimate of the induced E-field from a single-frequency sinusoid and that during the actual TMS waveform. That being the case, we employed the Fourier Solver to perform a frequency analysis in order to obtain the ratio of the E-field from a single-frequency component (e.g., 1000 Hz sinusoid) and that from the actual waveform. The Fourier Solver was an accurate and efficient method to compute the E-field during the TMS stimulus waveform.

Our results suggest that when modeling TMS, close attention should be given to the orientation of neural elements, the morphology of the cortical surface, and coil geometry. We found that rotating the coil 15° caused D-wave thresholds to change both inside and outside the target region, which suggests that locations of D-wave recruitment have an acute sensitivity to coil position and orientation. The fraction of neurons below total-mean threshold (the mean from all coil orientations combined) was quantified for each coil orientation (Fig. 9). These quantities suggest that a preferred coil orientation for the hand-knob target exists (~30°).

E-field maps indicate that focal stimulation of the hand-knob can be achieved with certain coil orientations. With E-field alone, however, it is difficult to predict whether untargeted areas are being avoided. For example, E-field maps (Fig. 5) show that coil orientations between +75° and +135° would be ineffective in stimulating the hand-knob, whereas orientations between 0° and 90° would be more effective. However, neuron excitability maps (Fig. 7) indicate that no coil orientation stimulates the hand-knob region while avoiding other regions.

We displayed E-field magnitudes on the cortical surface to point out the discrepancies with changing coil orientations (Fig. 8). The highly conductive CSF impacts the magnitude of the current density within the WM and GM, even though the magnetic field decays exponentially. Eichelbaum et al. (56) show that the current directionality and CSF are important in volume conduction, and this mechanism is likely responsible for the significant changes in E-field magnitude with changes in coil orientation.

Excitability maps (Fig. 7) from opposing (180° apart) coil orientations have noticeable differences, which do not appear in E-field maps. This discrepancy demonstrates the importance of time-dependent modeling to assess neural responses in areas of interest. Excitability maps illustrate the complexity of TMS and the inherent difficulty in constraining stimulation. The corollary is that the E-field, though simpler, does not provide an accurate prediction of stimulated brain regions according to our model. Our modeling technique could also validate motor-mapping procedures when dealing with large coil position datasets acquired from TMS navigation systems.

Physiological observations from Balslev et al. (57) and Dubach et al. (52) confirm observations from our model simulations. Dubach et al. report MEP latencies that suggest D-wave recruitment from TMS, so we compared their observations of the MEP amplitude relative to coil orientation with simulated thresholds of pyramidal cells. Our results indicate that more neurons within the hand-knob (black outline, Fig. 7) have low thresholds with coil orientations around 180° (when current flow is posterior at the stimulus onset). This observation agrees with Balslev et al. and Dubach et al. who found that the largest MEP amplitude was elicited with orientations that induced anteriorly directed current flow (this is the "posterior" orientation according to Balslev et al. and 165° according to Dubach et al.). Though our simulation results agree with previously published results, our model remains to be validated with TMS studies utilizing electrophysiology and TMS navigation simultaneously.

For each D-wave threshold map (Fig. 7), we quantified the overall effect of TMS by counting the number of pyramidal cell neurons that had a D-wave threshold below the mean threshold (from all maps combined) (Fig. 9). We recognize that this quantity is not a measure of the effectiveness of a certain TMS coil position as both targeted and untargeted areas are included in this quantification. Interestingly, this measure seems to coincide with the consensus in motor mapping applications: a coil angle of ~45° elicits robust responses in the hand-knob. However, the degree to which adjacent brain regions are affected seems significant, and our approach provides the means to test different coil geometries for stimulating specific neural structures while avoiding others. Lastly, broad threshold measures in Figure 9 show that the biphasic pulse has a lesser effect on pyramidal cell models underneath the coil for all orientations compared with the monophasic pulse for a given stimulus intensity. This dichotomy could possibly be explained in terms of the inherently greater E-fields induced by the monophasic waveform according to the setting on the dial of the stimulator units (1:0.6 ratio of max. E-field for monophasic to biphasic stimulation) (51). Both experimental and theoretical evidence show that thresholds are lower for the biphasic waveform (8), which was true for our model. Generally, the E-field intensity required to excite our pyramidal cell model was lower for biphasic stimulation compared with monophasic stimulation. This is likely due to the duration of the second phase of the biphasic waveform, which outlasts the phase of the monophasic pulse by almost 100 μsec. The duration of this second phase lasts approximately 190 μsec, and is more amenable to cause membrane depolarization.

CONCLUSION

Our results suggest that small changes in TMS parameters (i.e., TMS coil placement, TMS waveform, and head anatomy) can affect stimulation targets, and that these changes could result in variability in the location of energy delivery and the degree of neuromodulation within cortex. In addition, we have demonstrated that TMS navigation data combined with subject-specific modeling can be used to quantify the excitability of pyramidal cells around the targeted area. Our modeling approach enables the evaluation of a broad range of coil positions and orientations with only a single finite element mesh, which is advantageous when performing analysis on a per-pulse basis. Lastly, we found that accurately modeling the electromagnetic interactions within the brain requires close attention to: 1) the geometry of the cortex and WM surfaces; 2) the TMS parameters that are both fixed (coil winding geometry) and adjustable (coil position and orientation relative to the head); and 3) orientation of excitable neural elements in the cortex and WM.

Acknowledgements

The authors acknowledge funding from Clinical & Translational Science Institute of Southeast Wisconsin; Department of Neurology, Medical College of Wisconsin; and Department of Biomedical Engineering, Marquette University via Falk Foundation grant: "Collaborative Research Integrating Neuroimaging and Neurorehabilitation."

Authorship Statements

Drs. Goodwin and Butson conducted the study, including data collection and data analysis. Dr. Brian D. Goodwin prepared the manuscript draft with important intellectual input from Dr. Christopher R. Butson. All authors approved the final manuscript. Drs. Goodwin and Butson had complete access to the study data.

How to Cite this Article:

Goodwin B.D., Butson C.R. 2015. Subject-Specific Multiscale Modeling to Investigate Effects of Transcranial Magnetic Stimulation.
Neuromodulation 2015; 18: 694–704

REFERENCES

1. Rossi S, Hallett M, Rossini PM, Pascual-Leone A. Safety, ethical considerations, and application guidelines for the use of transcranial magnetic stimulation in clinical practice and research. *Clin Neurophysiol* 2009;120:2008–2039. doi: 10.1016/j.clinph.2009.08.016
2. Bortolomasi M, Minelli A, Fuggetta G et al. Long-lasting effects of high frequency repetitive transcranial magnetic stimulation in major depressed patients. *Psychiatry Res* 2007;150:181–186. doi: 10.1016/j.psychres.2006.04.010
3. Säisänen L, Könönen M, Julkunen P et al. Non-invasive preoperative localization of primary motor cortex in epilepsy surgery by navigated transcranial magnetic stimulation. *Epilepsy Res* 2010;92:134–144. doi: 10.1016/j.eplepsyres.2010.08.013
4. Nitsche MA, Paulus W. Noninvasive brain stimulation protocols in the treatment of epilepsy: current state and perspectives. *Neurother* 2009;6:244–250. doi: 10.1016/j.nurt.2009.01.003
5. Kleinjung T, Eichhammer P, Langguth B et al. Long-term effects of repetitive transcranial magnetic stimulation (rTMS) in patients with chronic tinnitus. *Otolaryngol Neck Surg* 2005;134:566–569. doi: 10.1016/j.otohns.2004.09.134
6. Williams JA, Imamura M, Fregni F. Updates on the use of non-invasive brain stimulation in physical and rehabilitation medicine. *J Rehabil Med* 2009;41:305–311. doi: 10.2340/16501977-0356
7. Sampson SM, Rome JD, Rummans TA. Slow-frequency rTMS reduces fibromyalgia pain. *Pain Med* 2006;7:115–118. doi: 10.1111/j.1526-4637.2006.00106.x
8. Di Lazzaro V, Ziemann U, Lemon RN. State of the art: physiology of transcranial motor cortex stimulation. *Brain Stimul* 2008;1:345–362. doi: 10.1016/j.brs.2008.07.004
9. Fregni F, Simon DK, Wu A, Pascual-Leone A. Non-invasive brain stimulation for Parkinson's disease: a systematic review and meta-analysis of the literature. *J Neurol Neurosurg Psychiatry* 2005;76:1614–1623. doi: 10.1136/jnnp.2005.069849
10. Hoogendam JM, Ramakers GMJ, Di Lazzaro V. Physiology of repetitive transcranial magnetic stimulation of the human brain. *Brain Stimul* 2010;3:95–118. doi: 10.1016/j.brs.2009.10.005
11. Jung NH, Delvendahl I, Kuhnke NG, Hauschke D, Stolle S, Mall V. Navigated transcranial magnetic stimulation does not decrease the variability of motor-evoked potentials. *Brain Stimul* 2010;3:87–94. doi: 10.1016/j.brs.2009.10.003
12. Herbsman T, Forster L, Molnar C et al. Motor threshold in transcranial magnetic stimulation: the impact of white matter fiber orientation and skull-to-cortex distance. *Hum Brain Mapp* 2009;30:2044–2055. doi: 10.1002/hbm.20649
13. Di Lazzaro V, Oliviero A, Pilato F et al. The physiological basis of transcranial motor cortex stimulation in conscious humans. *Clin Neurophysiol* 2004;115:255–266. doi: 10.1016/j.clinph.2003.10.009
14. Pashut T, Wolfus S, Friedman A et al. Mechanisms of magnetic stimulation of central nervous system neurons. *PLoS Comput Biol* 2011;7:e1002022. doi: 10.1371/journal.pcbi.1002022
15. Terao Y, Ugawa Y. Basic mechanisms of TMS. *J Clin Neurophysiol* 2002;19:322–343.
16. Hern J, Landgren S. Selective excitation of corticofugal neurones by surface-anodal stimulation of the baboon's motor cortex. *J Physiol* 1962;161:73–90.
17. Basser PJ, Roth BJ. Stimulation of a myelinated nerve axon by electromagnetic induction. *Med Biol Eng Comput* 1991;29:261–268.
18. Roth BJ, Basser PJ. A model of the stimulation of a nerve fiber by electromagnetic induction. *Biomed Eng IEEE Trans* 1990;37:588–597.
19. Caparelli E, Backus W, Telang F et al. Simultaneous TMS-fMRI of the visual cortex reveals functional network, even in absence of phosphene sensation. *Open Neuroimag J* 2010;4:100–110.
20. Krieg TD, Salinas FS, Narayana S, Fox PT, Mogul DJ. PET-based confirmation of orientation sensitivity of TMS-induced cortical activation in humans. *Brain Stimul* 2013;6:1–7. doi: 10.1016/j.brs.2013.05.007
21. Datta A, Bansal V, Diaz J, Patel J, Reato D, Bikson M. Gyri-precise head model of transcranial DC stimulation: improved spatial focality using a ring electrode versus conventional rectangular pad. *Brain Stimul* 2009;2:201–207. doi: 10.1016/j.brs.2009.03.005.Gyri
22. Butson CR, Cooper SE, Henderson JM, McIntyre CC. Patient-specific analysis of the volume of tissue activated during deep brain stimulation. *Neuroimage* 2007;34:661–670. doi: 10.1016/j.neuroimage.2006.09.034
23. Chen M, Mogul DJ. A structurally detailed finite element human head model for simulation of transcranial magnetic stimulation. *J Neurosci Methods* 2009;179:111–120. doi: 10.1016/j.jneumeth.2009.01.010
24. Rullmann M, Anwander A, Dannhauer M, Warfield SK, Duffy FH, Wolters CH. EEG source analysis of epileptiform activity using a 1 mm anisotropic hexahedra finite element head model. *Neuroimage* 2009;44:399–410. doi: 10.1016/j.neuroimage.2008.09.009
25. Silva S, Basser PJ, Miranda PC. Elucidating the mechanisms and loci of neuronal excitation by transcranial magnetic stimulation using a finite element model of a cortical sulcus. *Clin Neurophysiol* 2008;119:2405–2413. doi: 10.1016/j.clinph.2008.07.248
26. Miranda PC, Hallett M, Basser PJ. The electric field induced in the brain by magnetic stimulation: a 3-D finite-element analysis of the effect of tissue heterogeneity and anisotropy. *IEEE Trans Biomed Eng* 2003;50:1074–1085. doi: 10.1109/TBME.2003.816079
27. Güllmar D, Haueisen J, Reichenbach JR. Influence of anisotropic electrical conductivity in white matter tissue on the EEG/MEG forward and inverse solution. A high-resolution whole head simulation study. *Neuroimage* 2010;51:145–163. doi: 10.1016/j.neuroimage.2010.02.014
28. De. Lucia M, Parker GJM, Embleton K, Newton JM, Walsh V. Diffusion tensor MRI-based estimation of the influence of brain tissue anisotropy on the effects of transcranial magnetic stimulation. *Neuroimage* 2007;36:1159–1170. doi: 10.1016/j.neuroimage.2007.03.062
29. Opitz A, Windhoff M, Heidemann RM, Turner R, Thielscher A. How the brain tissue shapes the electric field induced by transcranial magnetic stimulation. *Neuroimage* 2011;58:849–859. doi: 10.1016/j.neuroimage.2011.06.069
30. Opitz A, Legon W, Rowlands A, Bickel WK, Paulus W, Tyler WJ. Physiological observations validate finite element models for estimating subject-specific electric field distributions induced by transcranial magnetic stimulation of the human motor cortex. *Neuroimage* 2013;81:253–264. doi: 10.1016/j.neuroimage.2013.04.067
31. Thielscher A, Opitz A, Windhoff M. Impact of the gyral geometry on the electric field induced by transcranial magnetic stimulation. *Neuroimage* 2011;54:234–243. doi: 10.1016/j.neuroimage.2010.07.061
32. Amatrudo JM, Weaver CM, Crimins JL, Hof PR, Rosene DL, Luebke JI. Influence of highly distinctive structural properties on the excitability of pyramidal neurons in monkey visual and prefrontal cortices. *J Neurosci* 2012;32:13644–13660. doi: 10.1523/JNEUROSCI.2581-12.2012
33. Edgley S, Eyre JA, Lemon RN, Miller S. Comparison of activation of corticospinal neurons and spinal motor neurons by magnetic and electrical transcranial stimulation in the lumbosacral cord of the anaesthetized monkey. *Brain* 1997;120:Pt 5.
34. Day BL, Dressler D, Maertens de Noordhout A et al. Electric and magnetic stimulation of human motor cortex: surface EMG and single motor unit responses. *J Physiol* 1989;412:449–473.
35. Salinas FS, Lancaster JL, Fox PT. Detailed 3D models of the induced electric field of transcranial magnetic stimulation coils. *Phys Med Biol* 2007;52:2879–2892. doi: 10.1088/0031-9155/52

36. Roth Y, Amir A, Levkovitz Y, Zangen A. Three-dimensional distribution of the electric field induced in the brain by transcranial magnetic stimulation using figure-8 and deep H-coils. *J Clin Neurophysiol* 2007;24:31–38. doi: 10.1097/WNP.0b013e31802fa393
37. Rotem A, Neef A, Neef NE et al. Solving the orientation specific constraints in transcranial magnetic stimulation by rotating fields. *PLoS ONE* 2014;9:e86794. doi: 10.1371/journal.pone.0086794
38. Tadel F, Baillet S, Mosher JC, Pantazis D, Leahy RM. Brainstorm: a user-friendly application for MEG/EEG analysis. *Comput Intell Neurosci* 2011;2011:879716. doi: 10.1155/2011/879716
39. Dale AM, Fischl B, Sereno MI. Cortical surface-based analysis: I. Segmentation and surface reconstruction. *Neuroimage* 1999;194:179–194.
40. Baumann B, Bornschlegl C, Krell D, Bogerts B. Changes in CSF spaces differ in endogenous and neurotic depression A planimetric CT scan study. *J Affect Disord* 1997;45:179–188.
41. Wagner T, Zahn M, Grodzinsky AJ, Pascual-leone A. Three-dimensional head model simulation of transcranial magnetic stimulation. *IEEE Trans Biomed Eng* 2004;51:1586–1598.
42. Dannhauer M, Lanfer B, Wolters CH, Knösche TR. Modeling of the human skull in EEG source analysis. *Hum Brain Mapp* 2011;32:1383–1399. doi: 10.1002/hbm.21114
43. Bastos JP, Nelson S. *Electromagnetic modeling by finite element methods*. New York: Marcel Dekker, Inc, 2003.
44. Pascual-Leone A, Valls-Solé J, Wassermann EM, Hallett M. Responses to rapid-rate transcranial magnetic stimulation of the human motor cortex. *Brain* 1994;117:Pt 4.
45. Stinear CM, Barber PA, Coxon JP, Verryt TS, Acharya PP, Byblow WD. Repetitive stimulation of premotor cortex affects primary motor cortex excitability and movement preparation. *Brain Stimul* 2009;2:152–162. doi: 10.1016/j.brs.2009.01.001
46. Vaalto S, Säisänen L, Könönen M et al. Corticospinal output and cortical excitation-inhibition balance in distal hand muscle representations in nonprimary motor area. *Hum Brain Mapp* 2011;32:1692–1703. doi: 10.1002/hbm.21137
47. Thickbroom GW, Byrnes ML, Edwards DJ, Mastaglia FL. Repetitive paired-pulse TMS at I-wave periodicity markedly increases corticospinal excitability: a new technique for modulating synaptic plasticity. *Clin Neurophysiol* 2006;117:61–66. doi: 10.1016/j.clinph.2005.09.010
48. Nowak LG, Bullier J. Axons, but not cell bodies, are activated by electrical stimulation in cortical gray matter. *Exp Brain Res* 1998;118:477–488. doi: 10.1007/s002210050304
49. Butson CR, McIntyre CC. Tissue and electrode capacitance reduce neural activation volumes during deep brain stimulation. *Clin Neurophysiol* 2005;116:2490–2500. doi: 10.1016/j.clinph.2005.06.023
50. Leuze CWU, Anwander A, Bazin P-L et al. Layer-specific intracortical connectivity revealed with diffusion MRI. *Cereb Cortex* 2014;24:328–339. doi: 10.1093/cercor/bhs311
51. Kammer T, Beck S, Thielscher A, Laubis-Herrmann U, Topka H. Motor thresholds in humans: a transcranial magnetic stimulation study comparing different pulse waveforms, current directions and stimulator types. *Clin Neurophysiol* 2001;112:250–258.
52. Dubach P, Guggisberg AG, Rösler KM, Hess CW, Mathis J. Significance of coil orientation for motor evoked potentials from nasalis muscle elicited by transcranial magnetic stimulation. *Clin Neurophysiol* 2004;115:862–870. doi: 10.1016/j.clinph.2003.11.033
53. Walsh V, Pascual-Leone A. *Transcranial magnetic stimulation: a neurochronometrics of mind*. Cambridge, MA: MIT Press, 2005.
54. Chaturvedi A, Butson CR, Lempka SF, Cooper SE, McIntyre CC. Patient-specific models of deep brain stimulation: influence of field model complexity on neural activation predictions. *Brain Stimul* 2010;3:65–67. doi: 10.1016/j.brs.2010.01.003
55. McRobbie D, Foster MA. Thresholds for biological effects of time-varying magnetic fields. *Clin Phys Physiol Meas* 1984;5:67–78.
56. Eichelbaum S, Dannhauer M, Hlawitschka M, Brooks D, Knösche TR, Scheuermann G. Visualizing simulated electrical fields from electroencephalography and transcranial electric brain stimulation: a comparative evaluation. *Neuroimage* 2014;101:513–530. doi: 10.1016/j.neuroimage.2014.04.085
57. Balslev D, Braet W, McAllister C, Miall RC. Inter-individual variability in optimal current direction for transcranial magnetic stimulation of the motor cortex. *J Neurosci Methods* 2007;162:309–313. doi: 10.1016/j.jneumeth.2007.01.021

COMMENTS

The clinical and research application of noninvasive brain stimulation continues to grow. The use of TMS for therapeutic treatments similarly continues to expand. However, the lack of understanding how these externally applied magnetic fields result in electrophysiological activation in the brain remains a critically important deficiency in the field. This paper helps to provide a computational analysis that may offer some insights that can improve the targeting and application of TMS for humans.

David Mogul, PhD
Chicago, IL, USA

***

In their paper "Subject-Specific Multiscale Modeling to Investigate Effects of Transcranial Magnetic Stimulation" Goodwin and Butson present a model of TMS including a realistic rendering of the induced electric field in the human brain and the resulting neural activation patterns in a population of some 2000 pyramidal neurons in the motor cortex for various coil orientations. The integration of a detailed multicompartmental model of a cortical pyramidal neuron including descending axons is arguably the most significant contribution of this paper. It takes TMS modeling beyond the electric field distribution, and in doing so joins a small handful of simulation studies of the effect of TMS on neural populations. A logical next step would be the integration of other neuron types in the model such as interneurons, which are also known to be directly stimulated by TMS. This type of modeling studies is very important for advancing the understanding and rational development of TMS paradigms. Indeed, at present, the field of TMS lags behind in modeling efforts compared to deep brain stimulation, for example, and can learn much from the latter.

Another innovative aspect of the paper is the use of Fourier decomposition coupled to a harmonic FEM solver to construct the electric field as a function of time for a specific coil current waveform. This approach is particularly relevant if the tissue impedances in the model are frequency dependent, for example if permittivity cannot be neglected, and hence the quasistatic approximation is not applicable. On the other hand, when the tissues are assumed to be purely resistive, as is typical for TMS simulations including this work by Goodwin and Butson, an alternative, simpler time-domain approach to scaling the harmonic electric field solution (1) could be deployed as follows.

The distribution of the peak electric field $\mathbf{E}'(\mathbf{x})$ as a function of spatial coordinates $\mathbf{x}$ is computed by a harmonic solver for an arbitrary TMS coil current amplitude I_0' and frequency f'. In the harmonic solution, the peak rate of change of the coil current is $2\pi f' I_0'$. For a given coil current waveform $I(t)$, the corresponding electric field spatial distribution as a function of both space and time t can therefore be obtained by scaling the harmonic solution,

$$\mathbf{E}(\mathbf{x},t)=\frac{\mathbf{E}'(\mathbf{x})}{2\pi f' I_0'}\frac{dI(t)}{dt}. \quad (1)$$

The coil current $I(t)$ can be measured or extracted from a circuit simulation of the TMS device.

Alternatively, if the coil current waveform is unavailable, the amplitude of the electric field pulse at $t = 0$ can be calculated by replacing dI/dt with V_0/L

$$\mathbf{E}(\mathbf{x},0)=\frac{\mathbf{E}'(\mathbf{x})}{2\pi f' I_0'}\frac{V_0}{L} \quad (2)$$

where V_0 is the voltage of the stimulator energy-storage capacitor at the beginning of the TMS pulse ($t = 0$) and L is the inductance of the coil including the cable. Conventionally, the strength of TMS pulses is reported with the value of V_0 as percentage of its maximum for the given stimulator. To add the temporal component of the electric field, its waveform can be measured with a search coil at a single point under the TMS coil (2). The measured electric field waveform is then normalized to unity at its initial peak ($t = 0$), yielding u(t). The time-dependent electric field can be reconstructed from the static distribution Equation (2) and u(t),

$$\mathbf{E}(\mathbf{x},t)=\mathbf{E}(\mathbf{x},0)u(t). \quad (3)$$

Both expressions (1) and (3) reflect the separability of the electric field solution into a spatial component and a temporal component under the quasistatic approximation (3).

Angel V. Peterchev, PhD
Durham, NC, USA

REFERENCES

1. Deng Z-D, Lisanby SH, Peterchev AV. Electric field strength and focality in electroconvulsive therapy and magnetic seizure therapy: a finite element simulation study. *J Neural Eng* 2011;8:016007.
2. Epstein CM, Schwartzberg DG, Davey KR, Sudderth DB. Localizing the site of magnetic brain stimulation in humans. *Neurology* 1990;40(4):666–670.
3. Roth BJ, Basser PJ. A model of the stimulation of a nerve fiber by electromagnetic induction. *IEEE Trans Biomed Eng* 1990;37(6):588–597.

Comments not included in the Early View version of this paper.

